

## DEFICIT OF WIDE BINARIES IN THE $\eta$ CHAMAELEONTIS YOUNG CLUSTER

ALEXIS BRANDEKER<sup>1</sup>, RAY JAYAWARDHANA, PARANDIS KHAVARI

Department of Astronomy and Astrophysics, University of Toronto, 50 St. George Street, Toronto, ON M5S 3H4, Canada

KARL E. HAISCH, JR.

Physics Department, Utah Valley State College, 800 West University Parkway, Orem, UT 84058-5999

AND

DIEGO MARDONES

Departamento de Astronomía, Universidad de Chile, Casilla 36-D, Santiago, Chile

Accepted by *ApJ*, October 23, 2019

### ABSTRACT

We have carried out a sensitive high-resolution imaging survey of stars in the young (6–8 Myr), nearby (97 pc) compact cluster around  $\eta$  Chamaeleontis to search for stellar and sub-stellar companions. Given its youth and proximity, any sub-stellar companions are expected to be luminous, especially in the near infrared, and thus easier to detect next to their parent stars. Here, we present VLT/NACO adaptive optics imaging with companion detection limits for 17  $\eta$  Cha cluster members, and follow-up VLT/ISAAC near-infrared spectroscopy for companion candidates. The widest binary detected is  $\sim 0''.2$ , corresponding to the projected separation 20 AU, despite our survey being sensitive down to sub-stellar companions outside  $0''.3$ , and planetary mass objects outside  $0''.5$ . This implies that the stellar companion probability outside  $0''.3$  and the brown dwarf companion probability outside  $0''.5$  are less than 0.16 with 95 % confidence. We compare the wide binary frequency of  $\eta$  Cha to that of the similarly aged TW Hydrae association, and estimate the statistical likelihood that the wide binary probability is equal in both groups to be  $< 2 \times 10^{-4}$ . Even though the  $\eta$  Cha cluster is relatively dense, stellar encounters in its present configuration cannot account for the relative deficit of wide binaries. We thus conclude that the difference in wide binary probability in these two groups provides strong evidence for multiplicity properties being dependent on environment. In two appendices we derive the projected separation probability distribution for binaries, used to constrain physical separations from observed projected separations, and summarize statistical tools useful for multiplicity studies.

*Subject headings:* binaries: general — stars: low-mass, brown dwarfs — stars: pre-main sequence — stars: planetary systems

### 1. INTRODUCTION

Most solar-type stars reside in binaries (Duquennoy & Mayor 1991), yet their formation is not well understood. It is generally accepted that most stars form in groups rather than in isolation (Adams & Myers 2001). Intriguingly, the multiplicity of young stars in many regions seems to be systematically higher than that of their main-sequence counterparts (e.g. Mathieu et al. 2000, and references therein). The reason for this multiplicity overabundance is not entirely understood, although two principal scenarios have been proposed. One is that the multiplicity fraction is sensitive to the initial conditions of the star formation process. That would imply that different regions show a variety of multiplicity properties, and indeed, there seems to be some evidence for the multiplicity fraction being anticorrelated with the stellar density of the region (Patience & Duchêne 2001). Another possibility is that young stars start out with a high fraction of multiples that subsequently are disrupted due to dynamical evolution (e.g. Reipurth 2000). Star-forming regions are generally too dispersed for binaries to be disrupted by interactions between members. The alternative is that many stars form not just in binaries, but in unstable higher-order multiples that

get disrupted with time, as indeed suggested by numerical simulations (Bate et al. 2002; Delgado-Donate et al. 2004). For a recent review on the current status of the field, see Duchêne et al. (2006).

The nearby (97 pc), young (6–8 Myr, Jilinski et al. 2005, and references therein)  $\eta$  Chamaeleontis cluster was found by the X-rays emitted from its members, as revealed by *ROSAT*, together with their common space motion, as revealed by *Hipparcos* (Mamajek et al. 1999). The cluster is mainly populated by late-type stars (K3-M6, see Table 1), and shows no evidence for extinction (Mamajek et al. 2000). These properties all contribute to make the cluster an excellent laboratory for investigating brown dwarf (BD) and planet formation, and their evolution (e.g. Song et al. 2004; Luhman 2004; Haisch et al. 2005; Lyo et al. 2006; Jayawardhana et al. 2006). In particular, using adaptive optics (AO) systems on large telescopes, it is possible to reach high contrast-ratio sensitivities close in, to detect any wide ( $> 0''.5$ ) companion down to planetary masses.

In a previous high-resolution survey using speckle interferometry and AO on 2.2–3.6 m telescopes, Köhler & Petr-Gotzens (2002) searched 13 members for companions ( $\eta$  Cha 1–12 and 15, see Table 1). They found two resolved binaries,  $\eta$  Cha 1 and  $\eta$  Cha 9, and one suspected unresolved binary,  $\eta$  Cha 12.  $\eta$  Cha 12 has also been suspected to be binary due to its elevation in color-magnitude diagrams (Lawson et al. 2001; Luhman & Steeghs 2004).

Electronic address: brandeker@astro.utoronto.ca

<sup>1</sup> Stockholm Observatory, AlbaNova University Centre, SE-106 91 Stockholm, Sweden

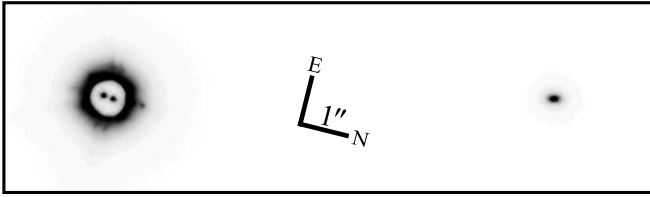


FIG. 1.— The close  $0''.2$  binary  $\eta$  Cha 1 observed with a semi-transparent coronagraphic mask, and a likely background object  $9''$  away (§ 4.1). The orientation and scale are shown by the two  $1''$  perpendicular axes..

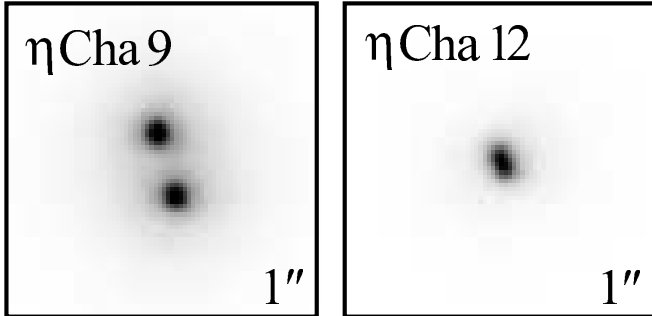


FIG. 2.— Close-ups of the tight binaries  $\eta$  Cha 9 (left) and  $\eta$  Cha 12 (right). The box sizes are  $1''$  on a side.  $\eta$  Cha 9 is a well resolved  $0''.2$  binary, while  $\eta$  Cha 12 is unresolved. From the asymmetric profile, we infer that the  $\eta$  Cha 12 separation is  $\sim 0''.04$  (§ 3.1). North is up, and east is to the left.

In the present paper we report on a deep AO search for faint companions to 17 confirmed members of the  $\eta$  Cha cluster. § 2 details the observations. § 3 describes analysis and results, including how astrometry and photometry were performed, how the Strehl ratio was measured and the contrast sensitivity estimated. In § 4 we discuss the companion candidates and constrain the orbit of the previously observed  $0''.2$  binary  $\eta$  Cha 1 (Fig. 1). We then go on to determine limits on the companion probability, use this to discuss the apparent deficit of binaries in the  $\eta$  Cha cluster, and estimate the likelihood of binaries being disrupted by stellar encounters. § 5 contains an enumerated list of conclusions.

In the Appendices, we first derive the (time-averaged) probability distribution for the projected separation of a binary, given its semi-major axis. We then continue with some useful properties of multiplicity statistics, in particular how to estimate binomial confidence intervals, and how to test if two outcomes are derived from the same binomial distribution.

## 2. OBSERVATIONS

We have observed 17 confirmed members of the  $\eta$  Cha cluster with high-resolution AO imaging and follow-up spectroscopy of companion candidates. Table 1 summarizes the observed target parameters and assigns a running target identification number used in this paper. Imaging data were obtained in service mode with the AO system NACO on the 8.2 m VLT Yepun at ESO (Cerro Paranal, Chile), during two different semesters (2002/2003 and 2004). Spectroscopic follow-up observations were obtained in service mode during 2004 using NACO and ISAAC (on VLT Antu).

For imaging with NACO, we used the high-resolution lens, giving a pixel scale of  $13.26 \text{ mas pix}^{-1}$  and the field of view  $13''.6 \times 13''.6$ . The full-width half maximums (FWHMs) of the diffraction limited point-spread functions (PSFs) of the setup in our used photometric bands  $J$  ( $1.27 \mu\text{m}$ ),  $H$  ( $1.66 \mu\text{m}$ ), and  $K_s$  ( $2.18 \mu\text{m}$ ) are 32 mas, 42 mas, and 56 mas, respectively. In the first semester, we obtained an extra exposure with a 5 mag neutral density filter for the stars we expected

would saturate the array during the minimum exposure time of 0.3454 s. In the second semester, we instead made use of the new semi-transparent coronagraphic mask for the brightest targets, that reduces the light within  $0''.35$  radius. We measured the contrast between the inside and outside of the mask to be  $6.0 \pm 0.1$  mag in  $H$  and  $6.3 \pm 0.1$  mag in  $K_s$ , by observing a binary with and without the coronagraphic plate. This is consistent with results found by the NACO instrument team (N. Ageorges, private communication). We used either the visual wave front sensor (WFS) mode VIS, or the infrared WFS modes N20C80 or N90C10, that direct 20% or 90% of the IR light to the WFS, and the rest to the science camera CONICA. The zenith seeing in the  $V$ -band was better than  $0''.6$  in general, though the targets, due to their low declination of  $-78^\circ$ , were observed at the relatively high air mass of 1.5–2.0. Three examples of obtained images are show in Figs. 1 & 2.

For spectroscopy with NACO, we used Grism 3 with the S27 lens, the N90C10 WFS, and a  $0''.086 \times 40''$  slit that produces an  $H$ -band spectrum from  $1.44 \mu\text{m}$  to  $1.72 \mu\text{m}$  at spectral resolution  $R \sim 1500$  and pixel scale  $27 \text{ mas pix}^{-1} \times 3.4 \text{ \AA pix}^{-1}$ .

For spectroscopy with ISAAC, we used the SWS1-LR mode with the  $SH$  filter, and a  $1'' \times 120''$  slit that produces an  $H$ -band spectrum from  $1.48 \mu\text{m}$  to  $1.80 \mu\text{m}$  at spectral resolution  $R \sim 500$  and pixel scale  $0''.148 \text{ mas pix}^{-1} \times 4.1 \text{ \AA pix}^{-1}$ .

The basic reduction was done in a standard way, making use of the reduction pipeline in the case of ISAAC. The sky was estimated from the jittered observations and subtracted from all frames, which were subsequently corrected for cosmic rays and flat fielded. Since the coronagraphic mask is in a fixed position on the array, half of the integration time was spent with the source chopped out of the field. For the spectroscopic observations, the slit was put over both primary and companion candidate, and then jittered along the slit. To decompose the spectra of two stars on the slit, we extracted the spectra by fitting two-component Moffat functions (Moffat 1969) to the spatial profiles. The wavelength calibration made use of Ar lamp spectra obtained during daytime. To correct for atmospheric absorption lines, an early type (B2–B5) telluric standard star was observed each night, at a similar airmass (within 0.2) to the target. The science spectra were then divided by the telluric standard spectra, multiplied by standard star models, and normalized. Unfortunately, the telluric line correction proved to not be entirely reliable, most probably due to the high airmass ( $\sim 2$ ) at which the observations were made.

The use of AO and a narrow slit makes the calibration of NACO spectra difficult. For example, the PSF, and therefore slit loss, varies with wavelength. In the NACO  $H$ -band spectra of the resolved  $\eta$  Cha 9 binary we noticed the spectral shape to be somewhat steeper than the ISAAC  $H$ -band spectrum we have for the unresolved binary. Since the observations were made at high airmass, we suspect this difference might be due to additional wavelength-dependent slit losses, caused by atmospheric differential refraction. To test this hypothesis we computed the expected atmospheric dispersion using the refraction index from Peck & Reeder (1972), and the standard dispersion equation (e.g., equation 3 in Roe 2002), giving the expected dispersion of 50 mas between  $1.5 \mu\text{m}$  and  $1.7 \mu\text{m}$ , which is a fair fraction of the 86 mas slitwidth. Projected on the slit orientation, the computed offset increases from 25 mas to 34 mas during the 10 exposures of  $\eta$  Cha 9, while at the same time the observed spectral slope gets steeper by  $\sim 15\%$ , indicating that differential refraction may indeed be signifi-

TABLE 1  
TARGETS OBSERVED IN THE  $\eta$  CHAMAELEONTIS CLUSTER

$\eta$ Cha <sup>a</sup>	Name	$\alpha_{J2000.0}$	$\delta_{J2000.0}$	$J$	$H$	$K_s$	SpT
1	EG Cha	08:36:56.24	-78:56:45.5	$8.155 \pm 0.019$	$7.498 \pm 0.049$	$7.338 \pm 0.021$	K4
2	$\eta$ Cha	08:41:19.48	-78:57:48.1	$5.688 \pm 0.019$	$5.721 \pm 0.040$	$5.718 \pm 0.018$	B8
3	EH Cha	08:41:37.03	-79:03:30.4	$10.349 \pm 0.023$	$9.647 \pm 0.022$	$9.415 \pm 0.019$	M3
4	EI Cha	08:42:23.72	-79:04:03.0	$9.535 \pm 0.024$	$8.779 \pm 0.061$	$8.615 \pm 0.019$	K7
5	EK Cha	08:42:27.11	-78:57:47.9	$10.777 \pm 0.023$	$10.099 \pm 0.021$	$9.855 \pm 0.021$	M5
6	EL Cha	08:42:38.80	-78:54:42.8	$10.232 \pm 0.027$	$9.584 \pm 0.023$	$9.290 \pm 0.021$	M2
7	EM Cha	08:43:07.24	-79:04:52.5	$8.420 \pm 0.024$	$7.758 \pm 0.034$	$7.635 \pm 0.033$	K3
8	RS Cha	08:43:12.23	-79:04:12.3	$5.994 \pm 0.030$	$5.877 \pm 0.038$	$5.852 \pm 0.034$	A7
9	EN Cha	08:44:16.38	-78:59:08.1	$10.260 \pm 0.026$	$9.668 \pm 0.026$	$9.335 \pm 0.024$	M4
10	EO Cha	08:44:31.88	-78:46:31.2	$9.653 \pm 0.023$	$8.919 \pm 0.063$	$8.732 \pm 0.021$	K7
11	EP Cha	08:47:01.66	-78:59:34.5	$8.729 \pm 0.020$	$8.025 \pm 0.055$	$7.655 \pm 0.038$	K4
12	EQ Cha	08:47:56.77	-78:54:53.2	$9.323 \pm 0.024$	$8.683 \pm 0.082$	$8.410 \pm 0.031$	M1
13	HD 75505	08:41:44.72	-79:02:53.1	$7.059 \pm 0.026$	$6.987 \pm 0.036$	$6.928 \pm 0.023$	A1V
15	ECHA J0843.3-7905	08:43:18.58	-79:05:18.2	$10.505 \pm 0.026$	$9.834 \pm 0.021$	$9.431 \pm 0.023$	M4
16	ECHA J0844.2-7833	08:44:09.15	-78:33:45.7	$12.505 \pm 0.024$	$11.976 \pm 0.022$	$11.618 \pm 0.024$	M5
17	ECHA J0838.9-7916	08:38:51.50	-79:16:13.7	$11.275 \pm 0.023$	$10.721 \pm 0.022$	$10.428 \pm 0.023$	M5
18	ECHA J0836.2-7908	08:36:10.73	-79:08:18.4	$11.849 \pm 0.024$	$11.277 \pm 0.026$	$10.945 \pm 0.021$	M5.5

NOTE. — Coordinates and IR magnitudes are from the 2MASS All Sky Data Release. The spectral types are from Mamajek et al. (1999) for 1–12, Houk & Cowley (1975) for 13, Lawson et al. (2002) for 15, and Song et al. (2004) for 16–18.

<sup>a</sup>Numbers 1–12 coincide with the RECX numbers introduced by Mamajek et al. (1999), and 1–18 with Luhman & Steeghs (2004). Their number 14 (“USNO Anon 1”) was not observed.

cant. The telluric standard was observed with the slit at the parallactic angle, and was thus not affected by differential refraction. These wavelength-dependent slit losses are of no consequence for the present observations, since we are interested in the spectral difference between the two components, but they might be of importance for future observations using VLT/NACO at high airmass.

Table 2 presents the observing log, with epochs, instrumentation, exposure time, and total integration time on source for each target.

### 3. ANALYSIS AND RESULTS

#### 3.1. Astrometry and photometry of sources in the field

For observations where multiple sources were well separated in the field, we measured the pixel positions on the array by making use of the `iraf` routine `imexamine`. To determine the relative precision of the astrometry we measured the separation between the tight, but well resolved, binary  $\eta$  Cha 1 for 10 different consecutive frames. The standard deviation was found to be about 0.12 pixels, or  $\sigma_{\text{std}} = 1.6$  mas. In addition, there is a systematic image scale uncertainty of  $\sigma_{\text{sc1}} \sim 0.01$  mas pix<sup>-1</sup>, so the estimated total separation error  $\sigma_{\text{sep}}$  depends on the separation  $s$  as  $\sigma_{\text{sep}}(s) = [(\sigma_{\text{sc1}}s)^2 + \sigma_{\text{std}}^2]^{1/2}$ . For some of the fainter sources,  $\sigma_{\text{std}}$  would be larger by a factor of several, due to poor centering.

The relative position angle error  $\sigma_{\text{PA}}$  was computed from  $\sigma_{\text{std}}$  by scaling the error with separation, i.e.  $\sigma_{\text{PA}}(s) = \arctan(\sigma_{\text{std}}s^{-1}) \approx \sigma_{\text{std}}s^{-1}$  rad. The position angle error is generally dominated by the systematic error of  $\sim 1^\circ$ , due to the uncertain orientation of the array. The astrometry is summarized in Table 3 & 4.

Photometric measurements of AO data are complicated by the spatially varying PSF. To estimate the level of anisoplanatism, we measured the PSF for the targets with multiple sources in the field. The FWHM of the PSF core (and thus the Strehl ratio) was found to be strongly dependent on the distance to the primary WFS. Out to a few arcseconds, the variation is less than 10%, but at larger separations ( $\gtrsim 7''$ ) the Strehl ratio can decrease by as much as a factor of 10. Part of the reason for this strong anisoplanatism may be that the stars were all observed at relatively high airmass ( $\eta$  Cha never rises

below an airmass of 1.5 from Cerro Paranal).

Because of the dependence of the PSF on separation, sources separated  $\gtrsim 4''$  from the primary have poorly constrained photometry. For those well-separated sources, we used a large aperture of 100 pixel radius for both the primary and secondary, if it was bright enough; otherwise we fit a Gaussian to the PSF core and computed the integrated flux under the Gaussian. Since the Strehl ratio is so low for the sources at large separation from the WFS star, their PSFs are reasonably well approximated by Gaussians. By using the Gauss-fitting procedure also on the bright wide companions, we found the two methods to be consistent within 0.3 mag, which is the quoted error. As a second consistency check we used the relatively bright source  $7''$  from  $\eta$  Cha 4, catalogued as  $H = 13.81 \pm 0.32$  by 2MASS, in agreement with our estimated  $H = 13.9 \pm 0.3$ .

For the close-in companions, where the PSF is roughly constant, we used aperture photometry with a radius of 4 pixels, and subtracted the background halo from the primary by measuring its brightness at the same separation but opposite position angle. The photometry is much more robust in this case. The error of the measured flux ratios is estimated by finding the consistency of multiple (consecutive) observations of the same target.

As the binary  $\eta$  Cha 12 is unresolved (Fig. 2), it requires special attention. We assume that the PSF core of the observation is circularly symmetric, as is the case for the other observed central PSFs, and that the elongation to the north east is the result of an equal mass binary. The position angle is then estimated from the position angle of an elliptical Gaussian fit, and the separation from the FWHM of the fit along and across the major axis, by computing their difference.

#### 3.2. Strehl ratios

The Strehl ratio  $S$  is defined as the ratio between the observed peak intensity  $P_{\text{obs}}$  of the PSF, and the theoretical peak intensity  $P_{\text{ideal}}$  of an idealized telescope (no distortion of wavefront, no obstructions) of the same aperture observing the same star,  $S \equiv P_{\text{obs}}/P_{\text{ideal}}$ . Instead of computing  $P_{\text{ideal}}$  for each observation, we estimated the ratio  $R_{\text{ideal}} = P_{\text{ideal}}/A_{\text{ideal}}$ , where  $A_{\text{ideal}}$  is the flux (integrated intensity), that only de-

TABLE 2  
OBSERVATION LOG

$\eta$ Cha <sup>a</sup>	UT Date	Instrument <sup>b</sup>	DIT (s)	Total (min)
1	2004-04-03	VIS <i>H</i> cor.	3	19
2	2004-04-04	VIS <i>H</i> cor.	3	15
3	2004-04-02	N90C10 <i>J</i>	20	13
3	2002-10-20	VIS <i>H</i>	0.6	15
3	2002-10-21	VIS <i>H</i>	0.6	14
3	2004-04-02	N90C10 <i>K<sub>s</sub></i>	20	27
4 B	2004-04-22	ISAAC <i>H</i> spec.	200	40
4	2002-11-17	VIS <i>H</i> ND	1.5	0.7
4	2002-11-17	VIS <i>H</i>	0.34	13
5	2003-01-17	N20C80 <i>H</i>	0.5	20
5	2003-01-21	N20C80 <i>H</i>	0.5	14
5	2003-02-17	N20C80 <i>H</i>	0.5	6
5	2003-02-19	N20C80 <i>H</i>	0.5	13
6	2003-01-18	VIS <i>H</i> ND	5	1.6
6	2003-01-18	VIS <i>H</i>	0.35	21
7	2004-04-04	VIS <i>H</i> cor.	20	20
8	2004-04-04	VIS <i>H</i> cor.	3	14
9	2004-04-02	N90C10 <i>J</i>	8	13
9	2003-01-21	VIS <i>H</i> ND	6	2
9	2003-01-21	VIS <i>H</i>	0.35	13
9	2004-04-02	N90C10 <i>K<sub>s</sub></i>	16	27
9 Aab	2004-04-03	N90C10 <i>H</i> spec.	120	40
9 B	2004-04-22	ISAAC <i>H</i> spec.	200	47
10	2003-01-22	VIS <i>H</i> ND	1.5	0.5
10	2003-01-22	VIS <i>H</i>	0.35	13
10 B	2004-04-24	ISAAC <i>H</i> spec.	200	60
11	2003-01-22	VIS <i>H</i> ND	1.2	0.4
11	2003-01-22	VIS <i>H</i>	0.35	13
12	2003-01-22	VIS <i>H</i> ND	1.5	0.5
12	2003-01-22	VIS <i>H</i>	0.35	13
13	2004-04-03	VIS <i>H</i> cor.	10	12
15	2004-04-02	N90C10 <i>J</i>	16	27
15	2003-01-21	VIS <i>H</i> ND	6	4
15	2003-01-21	VIS <i>H</i>	0.35	11
15	2003-01-22	VIS <i>H</i>	0.35	11
15	2004-04-02	N90C10 <i>K<sub>s</sub></i>	16	26
15 C	2004-04-22	ISAAC <i>H</i> spec.	200	40
16	2004-04-02	N90C10 <i>H</i>	80	36
17	2004-04-03	N90C10 <i>H</i>	10	33
18	2004-04-02	N90C10 <i>H</i>	30	33

<sup>a</sup> Letters refer to the companion candidate observed in addition to the primary.

<sup>b</sup> For NACO observations, VIS, N20C80 and N90C10 correspond to the used WFS, *J*, *H*, and *K<sub>s</sub>* are the used filters, ND means neutral density filter, cor. coronagraphic observations, and spec. spectroscopy. All ISAAC observation were made in the same mode (see § 2).

TABLE 3  
CONFIRMED COMPANIONS

$\eta$ Cha	Sep (")	PA <sup>a</sup> (°)	Band	FR <sup>b</sup>
1	0.192 ± 0.002	354.0 ± 0.3	<i>H</i>	1.15 ± 0.02
9	0.204 ± 0.003	195.7 ± 0.5	<i>J</i>	1.03 ± 0.04
9	0.207 ± 0.003	195.8 ± 0.5	<i>H</i>	0.96 ± 0.04
9	0.209 ± 0.003	196.4 ± 0.5	<i>K<sub>s</sub></i>	1.05 ± 0.04
12 <sup>c</sup>	0.040 ± 0.010	28 ± 4	<i>H</i>	1.0 ± 0.1

<sup>a</sup> The position angle is measured from north to east. There is an additional systematic error of  $\sim 1^\circ$ .

<sup>b</sup> The flux ratio A/B.

<sup>c</sup>  $\eta$  Cha 12 is unresolved, see § 3.1.

pends on telescope aperture and wavelength. For an 8.2 m telescope we computed  $R_J = 772 \text{ arcsec}^{-2}$ ,  $R_H = 452 \text{ arcsec}^{-2}$ , and  $R_{K_s} = 263 \text{ arcsec}^{-2}$ , for *J*, *H*, and *K<sub>s</sub>*, respectively. We then estimated similar ratios  $R_{\text{obs}} = P_{\text{obs}}/A_{\text{obs}}$  for the observations, and determined the Strehl ratio as  $S = R_{\text{obs}}/R_{\text{ideal}}$ . The peak intensity of the observed profile was found by fitting a circular Gaussian function to the PSF core, and the integrated

TABLE 4  
LIKELY CHANCE ALIGNMENT OBJECTS

$\eta$ Cha	Sep (")	PA <sup>a</sup> (°)	Band	Mag <sup>b</sup>
1 <sup>c</sup>	8.610 ± 0.018	13.8 ± 0.2	<i>H</i>	11.5 ± 1.0
2	7.997 ± 0.020	263.6 ± 0.2	<i>H</i>	19.8 ± 0.5
3	2.084 ± 0.005	106.5 ± 0.3	<i>J</i>	17.0 ± 0.5
3	2.034 ± 0.005	106.6 ± 0.3	<i>H</i>	16.3 ± 0.2
3	2.082 ± 0.005	106.1 ± 0.3	<i>K<sub>s</sub></i>	15.9 ± 0.2
4 <sup>d</sup>	7.352 ± 0.018	273.3 ± 0.2	<i>H</i>	13.9 ± 0.3
7	5.611 ± 0.016	344.2 ± 0.2	<i>H</i>	15.9 ± 1.0
8	9.443 ± 0.023	30.8 ± 0.2	<i>H</i>	17.4 ± 1.0
9 <sup>e</sup>	3.582 ± 0.010	141.7 ± 0.3	<i>J</i>	15.6 ± 0.2
9 <sup>e</sup>	3.526 ± 0.010	142.2 ± 0.3	<i>H</i>	15.3 ± 0.1
9 <sup>e</sup>	3.568 ± 0.010	141.8 ± 0.3	<i>K<sub>s</sub></i>	15.1 ± 0.1
10	9.895 ± 0.026	62.5 ± 0.2	<i>H</i>	16.6 ± 0.5
15 <sup>f</sup>	2.707 ± 0.040	73.4 ± 0.8	<i>J</i>	18.0 ± 0.5
15	2.726 ± 0.008	72.1 ± 0.3	<i>H</i>	17.5 ± 0.2
15 <sup>f</sup>	2.752 ± 0.040	72.7 ± 0.8	<i>K<sub>s</sub></i>	17.3 ± 0.5
15 <sup>g</sup>	6.370 ± 0.017	209.4 ± 0.2	<i>J</i>	13.8 ± 0.4
15	6.352 ± 0.017	210.0 ± 0.2	<i>H</i>	13.6 ± 0.2

<sup>a</sup> The position angle is measured from north to east. There is an additional systematic error of  $\sim 1^\circ$ .

<sup>b</sup> Apparent magnitudes were derived from Table 1.

<sup>c</sup> The astrometry was measured relative to the photocenter of the inner binary. This object is listed in 2MASS with  $J = 11.70 \pm 0.06$ ,  $H = 11.12 \pm 0.08$ , and  $K = 11.06 \pm 0.06$ , and in DENIS with  $I = 12.43 \pm 0.03$ .

<sup>d</sup> This object is listed in 2MASS as having  $J = 14.48 \pm 0.23$ ,  $H = 13.81 \pm 0.32$ , and  $K = 13.72 \pm 0.12$ .

<sup>e</sup> The astrometry was measured relative to the south component B of the inner binary.

<sup>f</sup> Marginal detection

<sup>g</sup> Object located at edge of array.

intensity by summing up all pixels within a circular aperture of  $2''$  radius.

The estimated Strehl ratios are shown in Figs. 3 & 4, except for the coronagraphic observations where we could not determine  $R_{\text{obs}}$  reliably, due to the presence of the mask. Because the coronagraphic targets are bright, and observed under similar conditions, we expect the Strehl ratios to be at the high end ( $>15\%$ ).

The lower the Strehl ratio, the larger fraction of the stellar flux that is diluted into the seeing disc. Even down to Strehl ratios of a few percent, however, there usually is a diffraction-limited core of the PSF. This means that searches for point sources (such as stars) are greatly aided by AO even at low Strehl ratios, while searches for extended structures (such as circumstellar material) are critically dependent on high Strehl ratios.

### 3.3. Contrast sensitivities

In order to estimate the sensitivity to companions as a function of separation, we used the following procedure:

1. For every pixel  $j$  in the detector, compute the distance  $r_j$  to the determined center of the primary.
2. Choose two radii  $R_0$  and  $R_1$  and fit an affine function  $f(r) = a_0 + a_1 r$ , where  $a_0$  and  $a_1$  are fitting constants, to the intensity  $I_j$  of all pixels  $j$  with  $r_j \in [R_0, R_1]$ . Reject pixels more than  $3\sigma$  from the fit.
3. Compute the standard deviation of the fit residuals,  $\sigma_{\text{pix}}(R) = \text{StdDev}[I_j - f(r_j)]$ , where  $R$  is the mean of all  $r_j \in [R_0, R_1]$ .
4. Measure the FWHM of the primary PSF, and the number of pixels  $N_{\text{PSF}}$  and integrated flux  $F_{\text{PSF}}$  within that area.

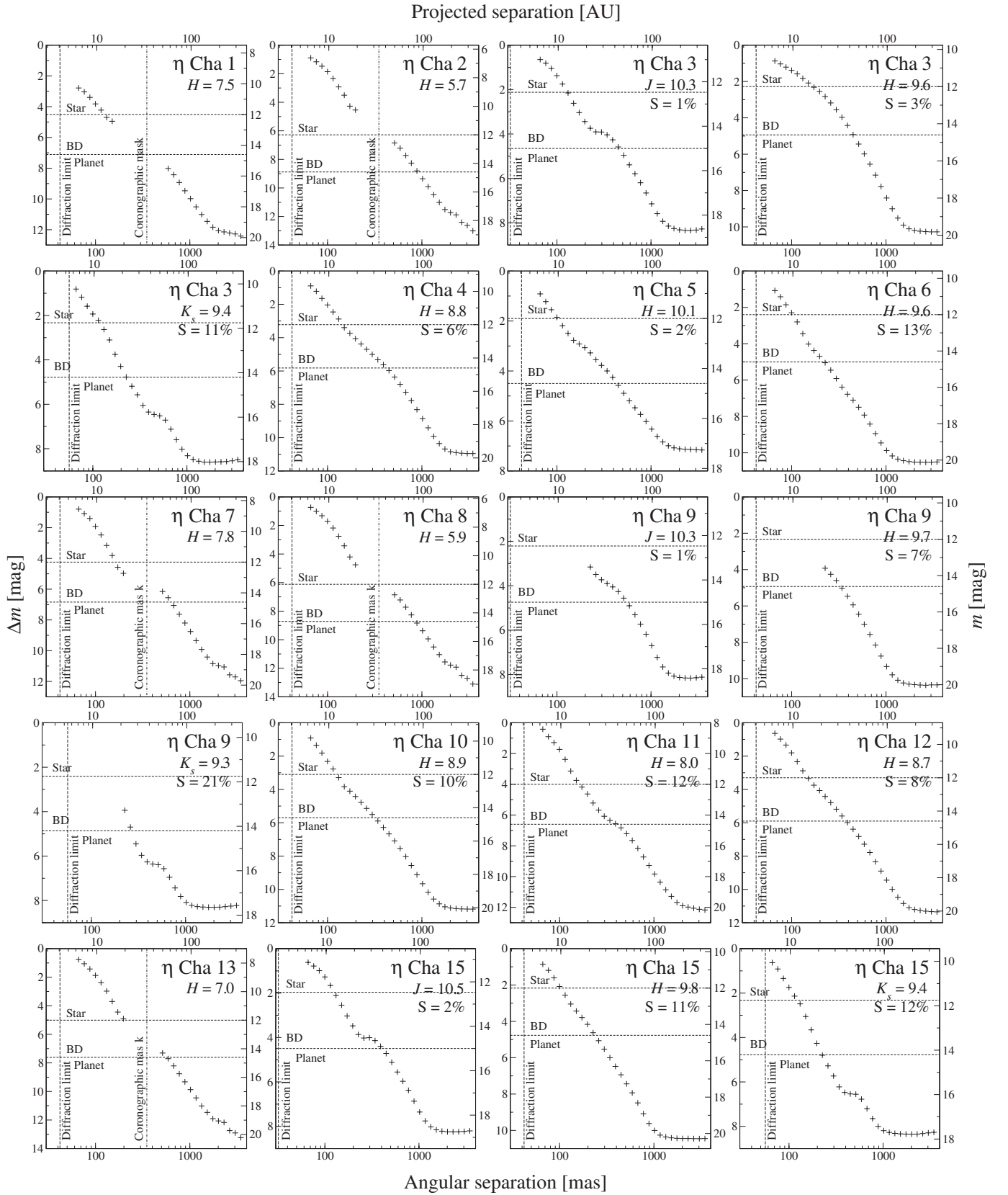


FIG. 3.— See the caption of Fig. 4.

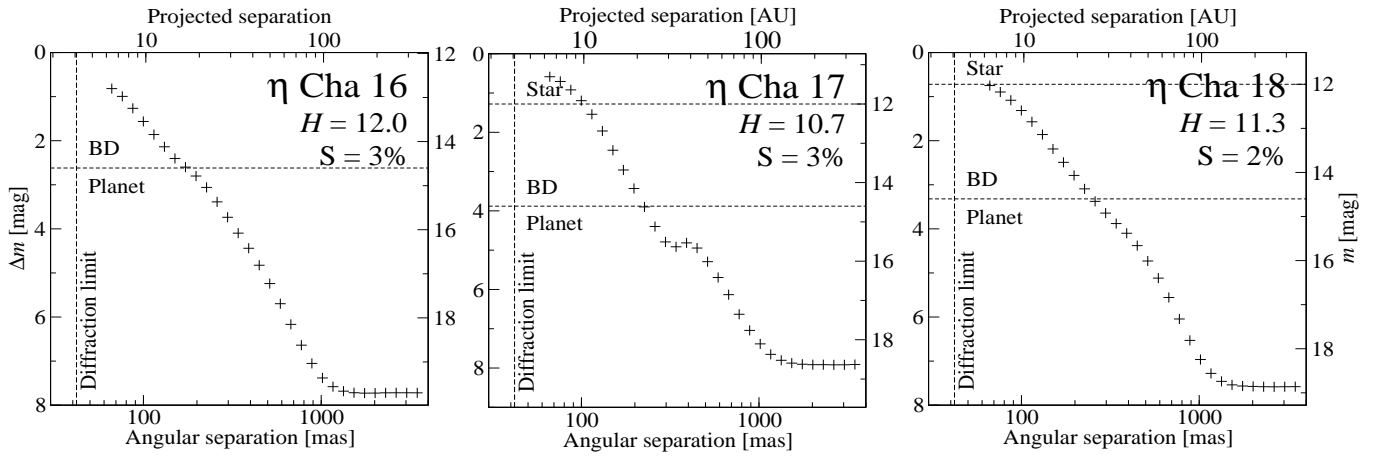


FIG. 4.— Sensitivity to companions as a function of separation, determined as described in § 3.3. The photometric band and magnitude is given in each panel, as well as the measured Strehl ratio (except for the coronagraphics observations, see § 3.2). Left vertical axes show the contrast sensitivity, while the right axes show the absolute sensitivity. The bottom horizontal axes show the angular separation and the upper axes the corresponding projected separation at the  $\eta$  Cha cluster distance of 97 pc. The diffraction limit and the semitransparent coronagraphic mask radius are shown as vertical dashed lines. The two horizontal dashed lines depict the star/brown dwarf ( $0.08 M_{\odot}$ :  $J = 12.5$ ,  $H = 12.0$ , and  $K = 11.8$ ) and brown dwarf/planetary mass ( $15 M_{J}$ :  $J = 15.0$ ,  $H = 14.6$ , and  $K = 14.2$ ) boundaries for the Baraffe et al. (2003) evolutionary models at age 8 Myr and distance 97 pc.

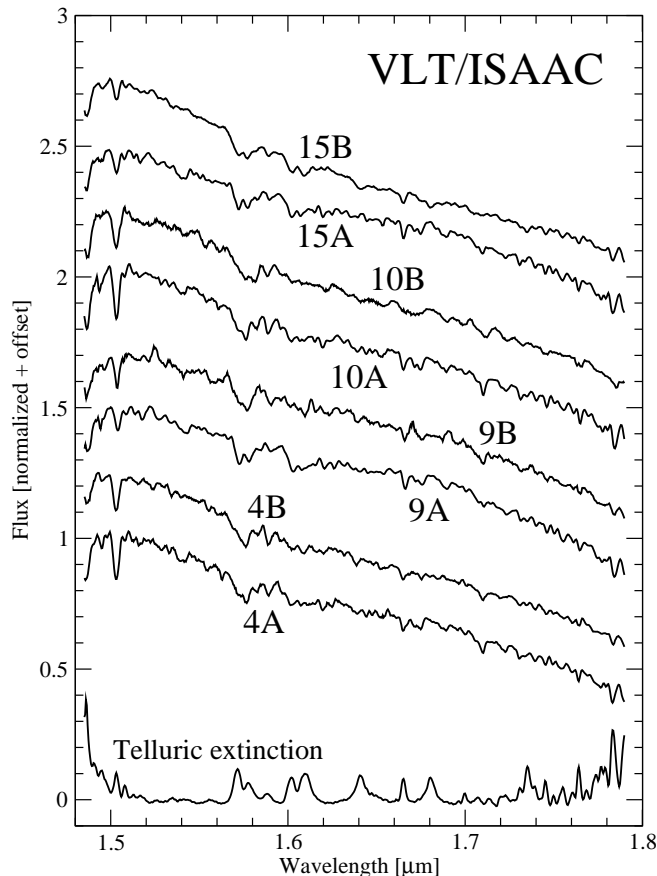


FIG. 5.— ISAAC spectra of the primaries and companion candidates of  $\eta$  Cha 4, 9, 10, and 15, denoted in the figure. The spectra have been normalized and offset in steps of 0.25. The lowest spectrum shows the telluric atmospheric extinction, also normalized and offset to 0. All of these companion candidates are likely background objects (§ 4.1).

5. The derived  $5\sigma$  contrast sensitivity is then estimated to be

$$\Sigma(R) = -2.5 \log_{10} \left[ \frac{5\sigma_{\text{pix}}(R)\sqrt{N_{\text{PSF}}}}{F_{\text{PSF}}} \right] \text{ mag.} \quad (1)$$

The *absolute* sensitivity is obtained by adding the primary magnitude to  $\Sigma(R)$ . The function  $f(r)$  in step 2 is fit to remove the radial gradient in the pixel intensities, that is due to the PSF. We confirmed that this procedure accurately estimates our achieved sensitivity by artificially placing intensity scaled PSFs at various separations. Since we limit the search to within  $5''$ , we do not correct for anisoplanatism (see § 3.1).

For the semi-transparent coronagraphic observations, we made use of the measured suppression ratio in  $H$  ( $6.0 \pm 0.1$  mag, § 2).

In the case of  $\eta$  Cha 9, which is a tight  $0''.2$  binary, we computed the contrast sensitivity from the center of light of the two stars, and estimated  $N_{\text{PSF}}$  and  $F_{\text{PSF}}$  as the average and sum, respectively, of both stars. The iso-intensity curves from the combined pair are elliptical rather than circular symmetric close to the stars, which is the reason the contrast sensitivity is estimated only at  $\geq 0''.2$  from the common center.

The contrast sensitivities for all observations are presented in Figs. 3 & 4.

### 3.4. Spectra of companion candidates

The obtained ISAAC  $H$ -band spectra of the primaries and companion candidates of the systems  $\eta$  Cha 4, 9, 10 and 15

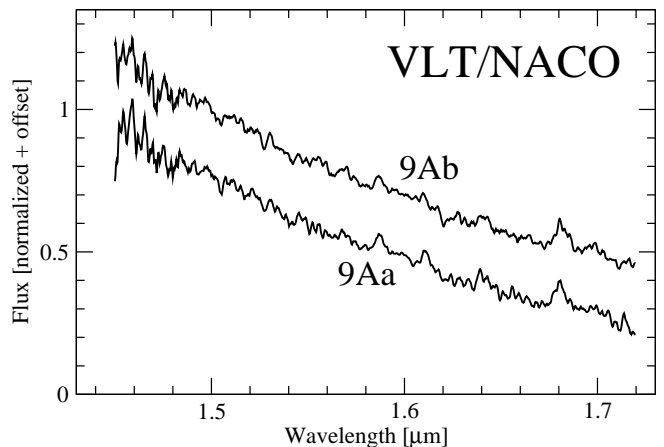


FIG. 6.— Resolved NACO spectra of the inner  $0''.2$   $\eta$  Cha 9 binary, normalized and offset by 0.25 from each other. The spectra are virtually identical. The scale has been chosen so that the flux scale / wavelength scale ratio is the same as in Fig. 5.

are shown in Fig. 5. Since the correction for telluric lines was poor due to high airmass, a plot of the extinction is also shown in Fig. 5. The NACO  $H$ -band spectrum of the inner  $0''.2$  binary of  $\eta$  Cha 9 is shown in Fig. 6.

## 4. DISCUSSION

### 4.1. Companion candidates

The  $\eta$  Cha cluster is only  $22^\circ$  from the Galactic plane, so the probability of chance alignment stars in the  $13''.6 \times 13''.6$  field of view is non-negligible. From the 2MASS All-Sky Data Release we find that the density of stars brighter than  $H \sim 16$  is  $\sim 10^{-3} \text{ arcsec}^{-2}$ , that statistically would produce about  $3 \pm 2$  chance alignments in our 17 fields, consistent with the total number of companion candidates (5) with  $H < 16$  in our sample. Since the observations are generally much more sensitive than this, we expect even more faint background stars. We have unfortunately no access to a deeper NIR survey of the region to find the local star density, but a general conclusion is that potentially *all* of the 10 new companion candidates found (Table 4) could be chance alignments.

For four of the candidates (near  $\eta$  Cha 4, 9, 10, and  $6''.4$  from  $\eta$  Cha 15) we have NIR ISAAC  $H$ -band spectra. If these companion candidates had been members of the  $\eta$  Cha cluster, their age ( $\sim 8$  Myr) and luminosity (from Table 4 and the distance 97 pc) would have implied very low-mass objects with atmospheres cooler than 2500 K (Baraffe et al. 2003), corresponding to spectral types later than M8.5 (Kirkpatrick et al. 1999; Luhman et al. 2003). This is clearly not the case, as the ISAAC spectra reveal all companion candidates to have spectral types equal to, or earlier than, their primaries (Fig. 5). In particular, there is no evidence for water depression that should be visible at  $\sim 1.5 \mu\text{m}$  for spectral types later than M5 (Cushing et al. 2005). We thus conclude that these companion candidates most likely are background stars, and not associated with the  $\eta$  Cha cluster.

For the companion candidate near  $\eta$  Cha 3, we have two epochs of data separated by 1.25 yr that show a relative position difference of  $(\Delta\alpha, \Delta\delta) = (48 \pm 7, -14 \pm 7)$  mas, implying a relative proper motion of  $(\mu_\alpha, \mu_\delta) = (38 \pm 6, -11 \pm 6)$  mas yr $^{-1}$ . A common proper motion is thus ruled out with  $> 5\sigma$ -significance, while the relative proper motion is roughly consistent with the companion candidate being a background star, since the proper motion of the  $\eta$  Cha cluster is  $(\mu_\alpha, \mu_\delta) =$

$(-30.0 \pm 0.3, 27.8 \pm 0.3)$  mas yr<sup>-1</sup> (Mamajek et al. 2000).

The inner companion candidate of  $\eta$  Cha 3 also has two epochs of data, but unfortunately the positional precision is not sufficient to significantly constrain the relative proper motion. The non-membership status of the star is instead revealed by its NIR colors; a  $H = 17.5$   $\eta$  Cha member should have had  $J-K \sim 3$  rather than  $J-K = 0.7 \pm 0.7$ .

The companion near candidate  $\eta$  Cha 1 is separated and bright enough to have 2MASS and DENIS photometry (Table 4). We reject this as a physical companion, since the observed  $I-(J,H,K)$  colors are  $\sim 1$  mag fainter than expected from the Baraffe et al. (1998) models, even when allowing for variability due to the epoch difference between 2MASS and DENIS.

The remaining 3 companion candidate stars (near  $\eta$  Cha 2, 7, and 8) have only single epoch  $H$ -band imaging, and therefore no direct way of ruling them out as physical companions. They are all quite distant from the system primary ( $> 5.6'' \sim 540$  AU) and faint ( $H \gtrsim 16$ ), however, and therefore likely chance alignments.

We conclude that, among the 17  $\eta$  Cha members surveyed, there are no detected companions with projected separations 20–500 AU.

#### 4.2. Orbit of $\eta$ Cha 1

Köhler & Petr-Gotzens (2002) used multi-epoch observations of  $\eta$  Cha 1 between 1996-03-29 and 2001-12-10 to compute a preliminary orbit, estimating a dynamical mass. With the additional data point from 2004-04-03, we can constrain the orbit further (see Fig. 7). In particular, among the two preferred orbits with periods of 43 yr and 151 yr found in Köhler & Petr-Gotzens (2002), the longer orbit is clearly favoured by our data. To possibly find a better orbital solution, we developed a simple orbit-fitting code that works as follows:

1. For a given orbit  $k$ , compute the positions  $(s_i^k, \phi_i^k)$  on sky for the dates of the observations, where  $s_i^k$  is the separation of orbit  $k$  and observation  $i$ , and  $\phi_i^k$  the corresponding position angle.
2. Compute the square sum  $\chi^2$  of the differences between the positions  $(s_i^k, \phi_i^k)$  from the assumed orbit, and the observed positions  $(s_i^{\text{obs}}, \phi_i^{\text{obs}})$ :

$$\chi^2(k) = \sum_{i=1}^N \left[ \left( \frac{s_i^k - s_i^{\text{obs}}}{\sigma_{s,i}} \right)^2 + \left( \frac{\phi_i^k - \phi_i^{\text{obs}}}{\sigma_{\phi,i}} \right)^2 \right],$$

where  $\sigma_{s,i}$  is the error in separation and  $\sigma_{\phi,i}$  the error in position angle (including estimated systematic errors).

3. Find the orbit  $k$  that minimizes  $\chi^2(k)$ .

The reason for using polar coordinates is that the position angle normally introduces a larger error than the separation, due to uncertainties in detector orientation.

While the 151 yr orbit of Köhler & Petr-Gotzens (2002) produces a good fit (Fig. 7), we find a multitude of very different orbits that produce equally good or better fits. In particular, there is a general solution degeneracy such that extremely eccentric orbits at high inclinations produce good fits (but with an unrealistically high system mass). An example is given in Fig. 7, where the unbroken line shows an orbit with a period of 93 yr and semi-major axis  $0''.416$ , corresponding to

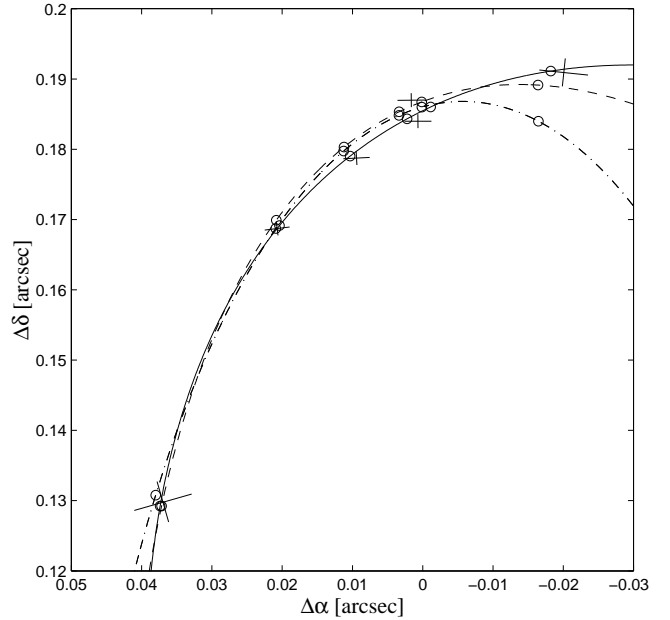


FIG. 7.— Relative astrometry between the two components of  $\eta$  Cha 1. The crosses show the measured separations, with the right-most data point coming from this paper and the others from Köhler & Petr-Gotzens (2002). The  $1\sigma$  positional errors are indicated by the size of the crosses. The dashed and dash-dotted curves are the orbit solutions found by Köhler & Petr-Gotzens (2002, see their Table 4), with periods of 150.8 yr and 42.5 yr, respectively. The unbroken line is the unphysical 93 yr period orbit fit mentioned in § 4.2. The small circles denote the positions in the orbits that correspond to the dates of the observations.

the system mass of  $7.6 M_{\odot}$  at the distance of 97 pc. Our conclusion is that the orbit has to be followed for a longer time span before useful limits on the dynamical mass can be made. Alternatively, spatially resolved radial velocity measurements would add valuable constraints.

#### 4.3. Limits on companion probability

The contrast sensitivity estimates from § 3.3 can be used to put limits on the number of likely companions. The basic approach is to assume that companions of stars are assigned by a stochastic process such that any given star system will have a companion with probability  $p$ , called the multiplicity (or binary) probability. The observed systems are then seen as a sample of this stochastic variable. Even if we knew with complete certainty that the 17 systems of  $\eta$  Cha had no wide stellar companions, there would still be a 5% chance that this outcome would have been produced with  $p = 0.16$ ; thus, the 95% confidence upper limit for  $p$  would have been 0.16.

Before we can do the proper statistics, however, we need to correct for the observational biases. That is, given that there is a companion, would we have detected it? Let  $p$  be the probability that a star has a companion, and  $q_j$  the probability that a companion would have been detected in system  $j$ , given that there had indeed been a companion there. Then the probability that a companion is not detected in system  $j$  is  $1 - pq_j$ , and the probability that no companions are detected in  $N$  systems enumerated from 1 to  $N$  is

$$\Phi(p) = \prod_{j=1}^N (1 - pq_j). \quad (2)$$

With a confidence set we mean the set of  $p$  such that  $\Phi(p) \leq 1 - \alpha$ , where  $\alpha$  is the chosen confidence, typically  $\alpha = 95\%$ . As  $\Phi(p)$  is a monotonously decreasing function of



$p$ , the confidence set becomes an interval  $[0, p_\alpha]$ , where we call  $p_\alpha$  the  $\alpha$ -confidence upper limit on  $p$ .

To derive  $p_\alpha$  we need to know  $q_j$  for all observed systems. For a given magnitude and separation from the star, this becomes straightforward using the contrast sensitivity estimates from § 3.3. If the brightness is above the sensitivity limit at the given separation in system  $j$ ,  $q_j = 1$ ; else  $q_j = 0$ . Equation 2 thus reduces to  $\Phi(p) = (1 - p)^n$ , where  $n$  is the number of systems where detection would have been possible. This implies  $p_\alpha = 1 - (1 - \alpha)^{1/n}$ . Because  $p_\alpha$  thus only depends on the discrete  $n$ ,  $p_\alpha$  will also be discrete, as shown in Fig. 8. In the left panel of Fig. 8 we derive 95% upper limits on the probability of companions of specific flux ratios to the primary, as a function of separation. To derive limits on the companion probability for specific mass ratios  $q$ , we assume primary masses from Lyo et al. (2004), and use evolutionary models from Baraffe et al. (2003) to translate companion mass to an  $H$ -band magnitude, assuming the age 8 Myr, distance 97 pc and solar metallicity. In the right panel of Fig. 8 we instead display limits on the absolute sensitivity to companions of different  $H$ -band magnitudes and masses.

From a physical point of view, rather than knowing the companion probability as a function of observed (projected) separation, it is more interesting to find the probability as a function of semi-major axis. To do that we need to know the probability  $q_j$  to find a companion, given that it has a specific semi-major axis. Our ability to detect a companion will depend on its projected distance to the primary, which in turn depends on viewing geometry and orbital phase (for eccentric orbits). In the Appendix, we compute the projected separation probability distribution for a companion of semi-major axis  $a$ . Assuming a random orientation, we derive the distribution analytically for circular orbits (§ A.1), and use a numerical approach in the case of eccentric orbits with an eccentricity distribution  $f(e) = 2e$  (motivated by both theory and observations; see § A.2). The probability  $q_j$  is then the probability that the companion is located at a detectable distance from the binary. Assuming that the sensitivity increases monotonously as a function of separation, this equals the probability that the companion is outside the “detection separation”  $d$  – i.e.

$$q_j = \int_{d/a}^{\infty} f_S(s) ds = 1 - F_S(d/a), \quad (3)$$

where  $f_S(s)$  is the projected separation probability density distribution found in the Appendix and shown in Fig. A1, and  $F_S(s)$  is the corresponding probability distribution. Since the projected separation can be arbitrary small for any semi-major axis, we always have that  $F_S(d/a) > 0$  for  $d/a > 0$ , and thus  $q_j < 1$ . Once we know  $q_j$ , equation 2 is used to compute 95% upper limits on the probability of companions. For the coronagraphic observations, the mask is at a fixed position only  $h = 2''5$  from the edge of the detector; we therefore introduce the additional correction factor  $g(s) = 1 - \pi^{-1} \arccos(h/s)$  (for  $s > h$ ) into the integral of equation 3, where  $g(s)$  is the probability that a companion at separation  $s$  is in the field of view.

In Fig. 9 we show the 95% upper limits in the same way as in Fig. 8, but as a function of the semi-major axes.

#### 4.4. Deficit of wide binaries

It is remarkable that, despite our high sensitivity, the *widest* binary detected in the  $\eta$  Cha cluster is only  $0''21$ , corresponding to the projected distance of 20 AU. This lack of wide binaries was already noted by Köhler & Petr-Gotzens (2002),

albeit with smaller statistics and less sensitive measurements. Outside 20 AU, we would have found any stellar companion (of mass  $> 0.07 M_\odot$ ; see Fig. 8). The fact that we do not detect any wide binaries among the 17 members implies that the wide ( $> 30$  AU) binary probability  $w_{\eta\text{Cha}}$  with  $1\sigma$  confidence is lower than  $p_{1\sigma} = 0.07$ , and with 95% confidence is lower than  $p_{95\%} = 0.18$  (Fig. 9). This stands in stark contrast to the other nearby, young (of the similar age 8 Myr) TW Hydrae association (TWA), where 11 out of the member stars TWA 1–19 are binaries with separations  $\gtrsim 30$  AU (Brandeker et al. 2003), corresponding to a wide binary probability of  $w_{\text{TWA}} = 0.58^{+0.13}_{-0.14}$ , clearly different from what we find in  $\eta$  Cha. This difference cannot be due to detection sensitivity differences; all the companions in TWA would have easily been detected in the  $\eta$  Cha cluster by this survey. The difference cannot be explained by small number statistics either, as the statistical likelihood that the  $\eta$  Cha cluster and TWA have binary frequencies drawn from the same distribution is less than  $2 \times 10^{-4}$  (see the Appendix).

There is certainly no deficiency of *close* binaries ( $< 30$  AU) in the  $\eta$  Cha cluster (Lyo et al. 2004). If anything, there might be a small over-abundance, compared to TWA, but the statistics are inconclusive.

One may speculate on the cause for such a difference in the wide binary population between the  $\eta$  Cha cluster and the TWA. One notable difference is that the  $\eta$  Cha cluster is much denser than the TWA. Could it be that wide binaries are dynamically disrupted in the  $\eta$  Cha cluster? To investigate this possibility we estimate the timescale for a binary to undergo a strong encounter with another star in the cluster. From Ivanova et al. (2005, equation 7), we have that this timescale is

$$\tau_{\text{coll}} = 1.7 \times 10^8 \text{ yr} \times \eta^2 k^{-2} n_5^{-1} \frac{\langle M \rangle^2}{M_1^2 M_2^2} \times \left( 1 + \eta \frac{2 M_1 + M_2 + \langle M \rangle}{k M_1 M_2} \langle M \rangle \right)^{-1}, \quad (4)$$

where  $\eta$  is the hardness of a binary,  $k \simeq 2$ ,  $n_5$  is the number density of star systems in units of  $10^5 \text{ pc}^{-3}$ ,  $\langle M \rangle$  is the mean mass per star system in units of  $M_\odot$ , and  $M_1$  and  $M_2$  are the masses of the binary components, also in units of  $M_\odot$ . The hardness of a binary is defined as

$$\eta = \frac{M_1 M_2}{\langle M \rangle \sigma^2 a} G M_\odot, \quad (5)$$

where  $G$  is the gravitational constant,  $a$  is the binary separation, and  $\sigma$  is the velocity dispersion of the cluster. Binaries with  $\eta < 1$  are termed soft, and those with  $\eta > 1$  hard. In general, soft binaries are disrupted by strong encounters, while hard binaries may survive. In the  $\eta$  Cha cluster, we have the cumulative mass  $16.6 M_\odot$  distributed over 17 systems (Lyo et al. 2004), giving  $\langle M \rangle = 1.0$ . There are presently no accurate radial velocities published for the  $\eta$  Cha members. However, from the estimated age of the cluster ( $\sim 8$  Myr) and observed effective radius ( $\sim 0.2$  pc), we infer that the cluster most likely is gravitationally bound. The present escape velocity is namely  $v_{\text{esc}} = (2GM/R)^{1/2} \sim 0.75 \text{ km s}^{-1}$ , assuming  $M = 13 M_\odot$  within  $R = 0.2$  pc (Lyo et al. 2004), which gives a crossing time of merely 0.3 Myr, enough to traverse the cluster core 25 times during its lifetime, while the relaxation time is only a few times the crossing time (Binney & Tremaine 1987, chapter 4). We therefore assume

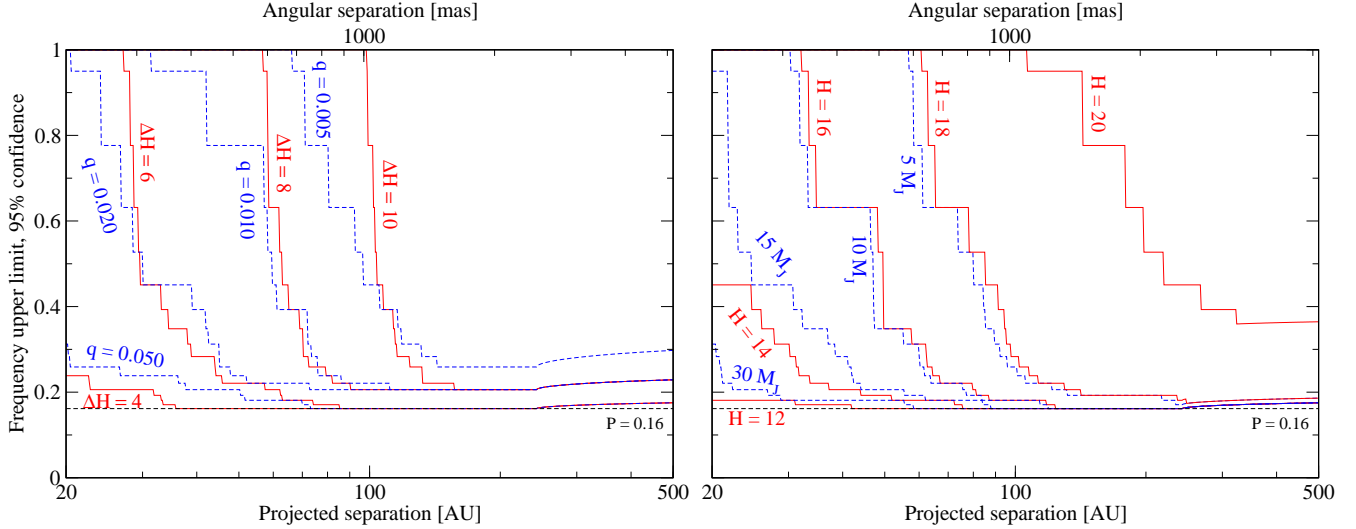


FIG. 8.— The 95% confidence upper limits on the probability of companions. The left panel shows the upper limits for companions of specific contrasts to the primary, as a function of separation from the star. The dashed lines (colored blue in electronic edition) show the sensitivity limits to mass ratios  $q = M_{\text{comp}}/M_{\text{prim}}$ , while the unbroken lines (colored red) show the limits for flux-ratios  $\Delta H$ . The right panel displays the absolute sensitivity, where the dashed lines (colored blue) show sensitivity to companion masses, and the unbroken lines (colored red) show the sensitivity to apparent  $H$ -band magnitudes. The dashed horizontal line shows the 95% confidence upper limit that would have been obtained statistically for our sample of 17 systems, had the detection sensitivity been 100%. The increased upper limits at separations  $>2''5$  is due to part of the field being outside the array.

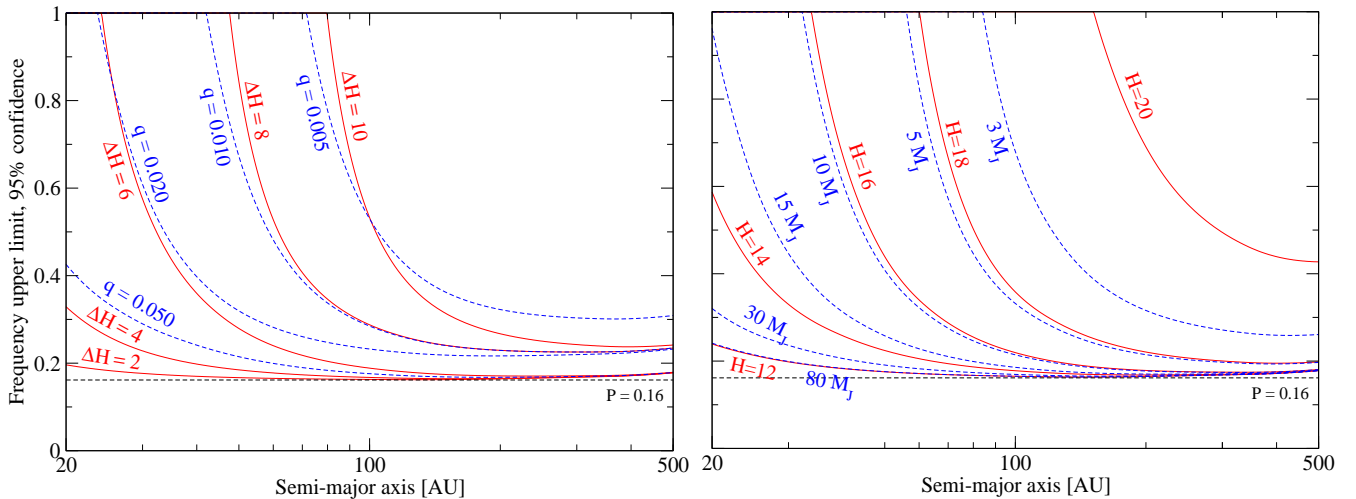


FIG. 9.— Same as in Fig. 8, except that the sensitivity limits are displayed as a function of semi-major axes, assuming the eccentricity probability density distribution  $f(e) = 2e$ .

$\sigma = v_{\text{esc}}/2 = 0.37 \text{ km s}^{-1}$ , in accordance with the virial theorem, implying that the condition for a binary to be soft in the  $\eta$  Cha cluster is  $a > 1600 \text{ AU} \gg 30 \text{ AU}$  for the typical masses  $M_1 = M_2 = 0.5$ . Moreover, for the  $\eta$  Cha cluster  $n_5 \sim 3 \times 10^{-3}$ , and the collision timescale for  $\eta = 1$  binaries is thus  $\tau_{\text{coll}} \sim 26 \text{ Gyr}$ , i.e. 3000 times longer than the lifetime of the system. That dynamical interactions between binaries in the present configuration of the cluster should be responsible for the lack of wide ( $>30 \text{ AU}$ ) binaries, consequently seems highly unlikely.

Since both the  $\eta$  Cha cluster and TWA are of similar age, the remaining explanation is that the difference in multiplicity properties were imprinted during the formation phase, as a result of different initial conditions. Either the groups formed with different multiplicity properties, or the properties dynamically evolved very early on, when the stars were possibly much closer together.

There seems to be a general trend that denser groups

have smaller wide binary frequencies than sparser regions; the sparse regions Taurus, Ophiuchus and Chamaeleon (Duchêne 1999), and MBM 12 (Brandeker et al. 2003) all have high wide binary frequencies, while the denser regions Trapezium (Petr et al. 1998), and NGC 2024, 2068, and 2071 (Padgett et al. 1997), have low wide binary frequencies. Solar-type main-sequence stars in the solar neighborhood have a binary probability of  $\sim 0.45$  (Leinert et al. 1993, and references therein), with half being wide (Duquennoy & Mayor 1991), and thus  $w_{\text{MS}} = 0.23$ , which is right in between  $w_{\eta \text{ Cha}}$  and  $w_{\text{TWA}}$ . It is therefore not clear from the wide binary statistics alone if sparse or dense star formation is the dominant mode – possibly both contribute equally. What is clear is that models of cluster formation and early evolution probably are essential to explain multiplicity properties (e.g. Bate et al. 2002; Delgado-Donate et al. 2004; Goodwin et al. 2006).

We summarize our conclusions as follows:

1. We found no new companions to stars in the  $\eta$  Cha cluster, despite being sensitive down to the star/BD limit outside  $0''.3$  (30 AU) and down to the BD/planet limit outside  $0''.5$  (50 AU).
2. We have constrained the orbit of  $\eta$  Cha 1 further, but are unable to usefully constrain a dynamical mass. Resolved radial velocities of the two components, or a longer astrometric time baseline, are required for an accurate mass estimate.
3. The 95 % upper limit for the wide ( $>30$  AU) binary probability  $w_{\eta\text{Cha}}$  in  $\eta$  Cha is  $p_{95\%}=0.18$ . This contrasts to the wide binary probability  $w_{\text{TWA}} = 0.58^{+0.13}_{-0.14}$  of TWA. The likelihood that  $w_{\eta\text{Cha}} = w_{\text{TWA}}$  is less than  $2 \times 10^{-4}$ .

4. Multiplicity properties depend on the initial conditions of the formation environment.

We acknowledge the outstanding support by the ESO user support department, in particular Sabine Mengel and Danuta Dobrzycka. We also thank Nancy Ageorges for help in determining the contrast of the semi-transparent mask. We are grateful to Marten van Kerkwijk, Natasha Ivanova and Serge Correia for valuable discussion. This research was supported by an NSERC grant and an SAO subcontract for the Keck Nuller project to RJ. We made extensive use of NASA's Astrophysics Data System Bibliographic Services, and the SIMBAD database and Vizier catalogue access tool, operated at CDS, Strasbourg, France. We used data products from the Two Micron All Sky Survey and the DENIS consortium.

*Facilities:* VLT:Yepun (NACO), VLT:Antu (ISAAC).

## APPENDIX

### A. PROBABILITY DISTRIBUTIONS FOR PROJECTED BINARY SEPARATIONS

This appendix concerns the computation of probability distributions of the observed projected separation between the two components of a binary system, given that the semi-major axis is known. Here we use the semi-major axis  $a$  of the companion orbit *relative to the primary*. If the mass of the companion is a significant fraction of the primary, this will be different from the semi-major axis  $a_{\text{com}}$  of the companion orbit relative to the center of mass. The relation is  $a = (M_{\text{comp}}/M_{\text{prim}} + 1)a_{\text{com}}$ , where  $M_{\text{comp}}$  and  $M_{\text{prim}}$  are the masses of the companion and primary, respectively. The derived probability distributions below are easily scaled to  $a_{\text{com}}$  in case of specific mass-ratio systems.

#### A.1. Companions in circular orbits

To compute the probability distribution for the projected separation of a companion, we need to make the assumption that the orbit is observed from a uniformly distributed direction; that is, any viewing direction is equally probable.

To generate a stochastic vector with a direction uniformly distributed over the unit sphere is a less trivial problem than one might naively expect. One cannot simply use a uniform distribution of spherical coordinates, since this would bias the vectors too much towards the poles; and one cannot simply use uniformly distributed Cartesian coordinates, since this would bias the directions towards the corners. Instead, a stochastic vector  $\mathbf{d} = (x, y, z)$  uniformly distributed over the unit sphere may be generated as

$$\begin{aligned} x &= \sqrt{1-z^2} \cos \phi \\ y &= \sqrt{1-z^2} \sin \phi \\ z &\in U(-1, 1), \end{aligned}$$

where  $X \in U(a, b)$  means that  $X$  is a stochastic variable uniformly distributed between  $a$  and  $b$ , and  $\phi \in U(0, 2\pi)$ . This is a corollary from a theorem by Archimedes, that states that a lateral area of a section cut out of a sphere by two parallel planes equals  $A = 2\pi Rh$ , where  $R$  is the radius of the sphere and  $h$  is the distance between the planes.

With  $\mathbf{R}$  being the radius vector from the star to the companion,  $R$  its length and  $\mathbf{d}$  the unit viewing direction vector, the projected distance between the star and the planet onto a plane perpendicular to the viewing direction will be  $s = \sqrt{R^2 - (\mathbf{R} \cdot \mathbf{d})^2}$ .

Since  $\mathbf{d}$  is uniformly distributed on the unit sphere, we can (without loss of generality) let  $\mathbf{R} = R\mathbf{e}_z$ , where  $\mathbf{e}_z$  is the unit vector along the  $z$ -axis. The scalar product becomes  $\mathbf{R} \cdot \mathbf{d} = Rd_z$ , where  $d_z$  is the  $z$ -component of the direction vector  $\mathbf{d}$ . That is, the scalar product is only dependent on the  $z$ -component of the direction vector:

$$s = R\sqrt{1-d_z^2}. \quad (\text{A1})$$

The probability distribution for the corresponding stochastic variable  $S = \sqrt{1-D^2}$ , where  $D \in U(0, 1)$ , becomes  $F_S(s) = 1 - \sqrt{1-s^2}$ , and the probability density distribution  $f_S(s) = dF_S(s)/ds = s/\sqrt{1-s^2}$ .

These distributions thus describe the projected separation  $s$ , in units of the orbital radius, of a companion in a circular orbit around a star (Fig. A1).

#### A.2. Companions in elliptical orbits

To derive the projected separation distribution for elliptical orbits is slightly more complicated than for circular motion, since the radial distance between the star and its companion is non-linear in time. We also have to make an additional assumption on the eccentricity distribution. We still do not have to bother with the orbital elements concerning a specific orientation of an orbit however, since we already have assumed that the viewing direction is random.

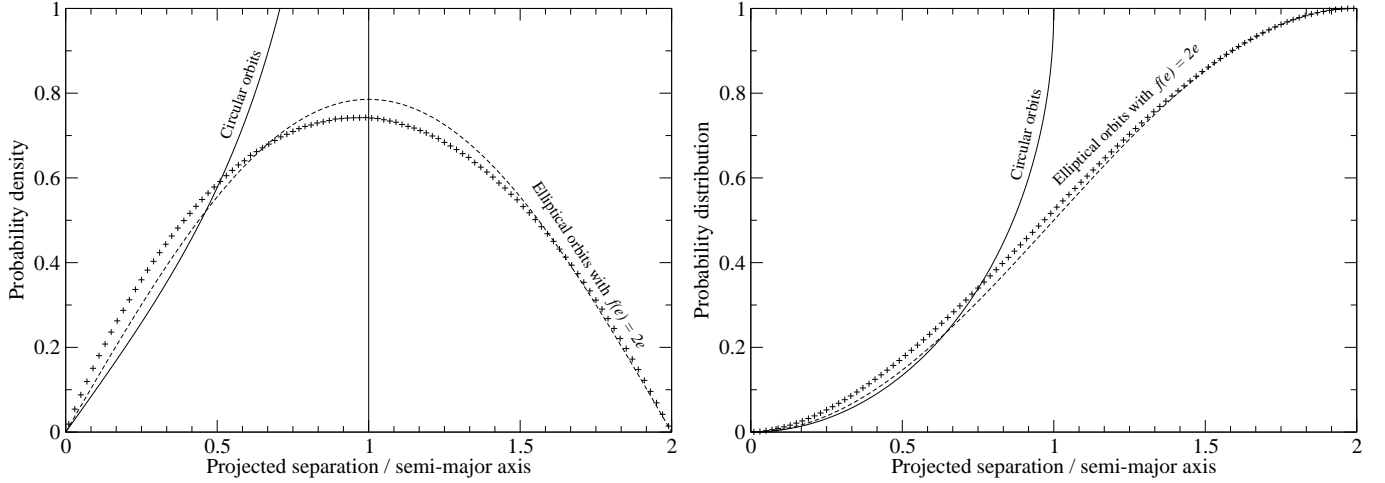


FIG. A1.— The left panel shows the probability density distribution for the projected separation of a companion to a star, in units of its semi-major axis. Two cases are plotted, one where the orbits are assumed to be circular (solid line), and one where the eccentricity density distribution is assumed to be  $f(e) = 2e$  (crosses). The projected separation distribution is computed exactly for circular orbits, and by a monte carlo approach for the eccentric orbits. The dashed line is an approximate fit, as outlined in § A.2. The right panel shows the corresponding probability distribution, i.e. the integral over the probability density.

The mean anomaly  $M$  of an elliptical orbit is defined to be linearly increasing with time (Meeus 1991, Chapter 29). Its relation to the eccentric anomaly  $E$ , that is used to compute the actual position of the companion, is defined by the Kepler equation  $E = M + e \sin E$ , where  $e$  is the eccentricity of the orbit. Since the Kepler equation is transcendental it cannot be solved algebraically, which complicates the analysis. We therefore derive the probability density distribution using the following monte carlo approach instead.

1. Let the mean anomaly  $M \in U(0, 2\pi)$ .
2. Get the eccentricity  $e$  from some pre-defined distribution  $f(e)$ .
3. Solve Kepler's equation numerically and compute the eccentric anomaly  $E(M)$ .
4. Compute the instantaneous distance between star and companion,  $R = 1 - e \cos E$ .
5. Let the projection term  $d_z \in U(-1, 1)$ , in line with equation A1, and compute the projected separation  $s = R\sqrt{1 - d_z^2}$ .

The choice of eccentricity distribution is important for the resulting probability density distribution. Theoretical considerations (Ambartsumian 1937) predict the distribution  $f(e) = 2e$ , where  $e \in [0, 1]$ , which is reasonably confirmed by observations of long-period binaries ( $> 1000$  days; Duquennoy & Mayor 1991). To generate a stochastic variable with  $f(e) = 2e$ , we let  $e = X^{1/2}$ , where  $X \in U(0, 1)$ . The result from a simulation of  $10^8$  binaries is shown in Fig. A1. The probability density distribution is well approximated, although not perfectly, by the function

$$f_S(s) = \frac{\pi}{4} \sin\left(\frac{\pi}{2}s\right), \quad (\text{A2})$$

where  $s \in [0, 2]$ , which is over plotted in Fig. A1. The corresponding probability distribution is

$$F_S(s) = \frac{1}{2} \left[ 1 - \cos\left(\frac{\pi}{2}s\right) \right]. \quad (\text{A3})$$

A stochastic variable  $S$  with this distribution can be generated from  $X \in U(0, 1)$  by setting  $S = 2\pi^{-1} \arccos(1 - 2X)$ , that might prove useful for future completeness studies.

## B. MULTIPLICITY STATISTICS

Statistical estimates of multiplicity frequencies are often limited by small sample numbers, where approximate methods using assumptions of Poisson or normal statistics become insufficient. Instead, more accurate estimates can be obtained by explicit use of binomial statistics. The multiplicities of  $N$  systems of a stellar association are viewed as outcomes  $x_i$  of a binomially distributed stochastic variable  $X \in \text{Bin}(1, p)$ , where  $p$  is the multiplicity probability for any specific system.  $x_i = 1$  if system  $i$  is multiple, and  $x_i = 0$  if not. The number of multiple systems is then  $k = \sum_i x_i$ , which in itself can be seen as the outcome of a binomially distributed stochastic variable  $K \in \text{Bin}(N, p)$ . The goal is to constrain  $p$  from a given set  $\{x_i\}$ , assuming all  $x_i$  are drawn from the same distribution. Here we summarize results from two outstanding problems, how to constrain the multiplicity probability  $p$  by a confidence interval, and how to decide if two sets  $\{x_i\}$  and  $\{y_i\}$  are outcomes of the same binomial distribution.

## B.1. Binomial confidence intervals

The well-known maximum-likelihood estimator of  $p$  is  $\hat{p} = \sum_i x_i / N$ , but to compute an accurate variance of this estimator is much more difficult. The most widely used way of computing the standard deviation of  $\hat{p}$  is by using the so-called *Wald* method, that has the simple form  $\sigma = (\hat{p}(1-\hat{p})/N)^{1/2}$ . The Wald standard deviation produces very poor approximations whenever  $p$  is close to 0 or 1, however, and its usage is generally not recommended (Brown et al. 2001). The problem of computing accurate confidence intervals for the binomial distribution is not a new one, and there exist a plenitude of literature on the subject (see Brown et al. 2001 for a review of methods). A robust “exact” method guaranteed to produce intervals with confidence of *at least*  $\alpha$  was proposed by Clopper & Pearson (1934). If  $K \in \text{Bin}(N, p)$ , the probability that an outcome is  $k$  is  $P(k \text{ of } N) = \binom{N}{k} p^k (1-p)^{N-k}$ , and the probability that  $k < n \leq N$  is  $P(k < n \text{ of } N) = \sum_{k=0}^{n-1} P(k \text{ of } N)$ . For any given significance  $\alpha$  and specific outcome  $k$ , the Clopper-Pearson method consists of finding the interval  $(p_{\min}, p_{\max})$  such that if  $p \geq p_{\min}$ , then  $P(j < k \text{ of } N) \leq (1-\alpha)/2$ , and if  $p \leq p_{\max}$ , then  $P(j > k \text{ of } N) \leq (1-\alpha)/2$ . By solving for the equalities, we get

$$\sum_{j=0}^k \binom{N}{j} p_{\min}^j (1-p_{\min})^{N-j} = \frac{1-\alpha}{2} \quad (\text{B1})$$

$$\sum_{j=0}^{k-1} \binom{N}{j} p_{\max}^j (1-p_{\max})^{N-j} = \frac{1+\alpha}{2}, \quad (\text{B2})$$

where we have used that  $P(j > k \text{ of } N) = 1 - P(j < k+1 \text{ of } N)$ . The equations B1 & B2 are normally best solved numerically.<sup>2</sup> In the degenerate case where  $k = 0$  or  $k = N$ , the confidence interval becomes one-sided, and the equations B1 & B2 are easily solved analytically (e.g., equation 2 in § 4.3).

## B.2. Comparing binomial distributions

Let  $k_A$  out of  $N_A$  systems in association  $A$  be multiple, and  $k_B$  out of  $N_B$  systems in association  $B$ . The question that naturally arises is, is the multiplicity probability  $p_A$  of system  $A$  similar to  $p_B$  of system  $B$ ? As in the case of binomial confidence intervals, there are several tests available in the literature (see Storer & Kim 1990 for a review). A conservative “exact” hypothesis test is based on Fisher (1935), where the hypothesis that  $p_A = p_B$  is tested: Let  $h(k_A, k_B, N_A, N_B) = \binom{N_A}{k_A} \binom{N_B}{k_B} / \binom{N_A+N_B}{k_A+k_B}$  and  $I[\text{expression}]$  be the indicator function that is 1 if *expression* is true, and 0 otherwise. Then the test function is

$$T = \sum_{x=\max(0, k_A+k_B-N_B)}^{\min(n_A, k_A+k_B)} h(x, k_A+k_B-x, n_A, n_B) \times I[h(x, k_A+k_B-x, n_A, n_B) \leq h(k_A, k_B, n_A, n_B)], \quad (\text{B3})$$

and the hypothesis is rejected if  $T \leq \alpha$ , where  $\alpha$  is the significance of the test. As an example, if  $k_A = 0$ ,  $N_A = 17$ ,  $k_B = 11$ , and  $N_B = 19$ , then  $T = 1.46 \times 10^{-4}$ , which is the quoted likelihood that the wide binary probability is equal in  $\eta$  Cha and TWA (§ 4.4).

## REFERENCES

- Adams, F. C., & Myers, P. C. 2001, *ApJ*, 553, 744  
 Ambartsumian, V. A. 1937, *Astron. Zh.*, 14, 207  
 Baraffe, I., Chabrier, G., Allard, F., & Hauschildt, P. H. 1998, *A&A*, 337, 403  
 Baraffe, I., Chabrier, G., Barman, T. S., Allard, F., & Hauschildt, P. H. 2003, *A&A*, 402, 701  
 Bate, M. R., Bonnell, I. A., & Bromm, V. 2002, *MNRAS*, 336, 705  
 Binney, J., & Tremaine, S. 1987, *Galactic dynamics* (Princeton, NJ, Princeton University Press, 1987, 747 p.)  
 Brandeker, A., Jayawardhana, R., & Najita, J. 2003, *AJ*, 126, 2009  
 Brown, L. D., Cai, T. T., & DasGupta, A. 2001, *Statistical Science*, 16, 101  
 Clopper, C. J., & Pearson, E. S. 1934, *Biometrika*, 26, 404  
 Cushing, M. C., Rayner, J. T., & Vacca, W. D. 2005, *ApJ*, 623, 1115  
 Delgado-Donate, E. J., Clarke, C. J., Bate, M. R., & Hodgkin, S. T. 2004, *MNRAS*, 351, 617  
 Duchêne, G. 1999, *A&A*, 341, 547  
 Duchêne, G., Delgado-Donate, E., Haisch, K., Loinard, L., & Rodriguez, L. 2006, *Protostars and Planets V*, preprint available at astro-ph/0603004  
 Duquenois, A., & Mayor, M. 1991, *A&A*, 248, 485  
 Fisher, R. A. 1935, *Journal of the Royal Statistical Society*, 25, 295  
 Goodwin, S. P., Whitworth, A. P., & Ward-Thompson, D. 2006, *A&A*, 452, 487  
 Haisch, K. E., Jayawardhana, R., & Alves, J. 2005, *ApJ*, 627, L57  
 Houk, N., & Cowley, A. P. 1975, *Michigan Catalogue of two-dimensional spectral types for the HD star* (Ann Arbor: University of Michigan, Departement of Astronomy, 1975)  
 Ivanova, N., Belczynski, K., Fregeau, J. M., & Rasio, F. A. 2005, *MNRAS*, 358, 572  
 Jayawardhana, R., Coffey, J., Scholz, A., Brandeker, A., & van Kerkwijk, M. H. 2006, *ApJ*, submitted
- Jilinski, E., Ortega, V. G., & de la Reza, R. 2005, *ApJ*, 619, 945  
 Kirkpatrick, J. D., Reid, I. N., Liebert, J., Cutri, R. M., Nelson, B., Beichman, C. A., Dahn, C. C., Monet, D. G., Gizis, J. E., & Skrutskie, M. F. 1999, *ApJ*, 519, 802  
 Köhler, R., & Petr-Gotzens, M. G. 2002, *AJ*, 124, 2899  
 Lawson, W. A., Crause, L. A., Mamajek, E. E., & Feigelson, E. D. 2001, *MNRAS*, 321, 57  
 —. 2002, *MNRAS*, 329, L29  
 Leinert, C., Zinnecker, H., Weitzel, N., Christou, J., Ridgway, S. T., Jameson, R., Haas, M., & Lenzen, R. 1993, *A&A*, 278, 129  
 Luhman, K. L. 2004, *ApJ*, 616, 1033  
 Luhman, K. L., Stauffer, J. R., Muench, A. A., Rieke, G. H., Lada, E. A., Bouvier, J., & Lada, C. J. 2003, *ApJ*, 593, 1093  
 Luhman, K. L., & Steeghs, D. 2004, *ApJ*, 609, 917  
 Lyo, A.-R., Lawson, W. A., Feigelson, E. D., & Crause, L. A. 2004, *MNRAS*, 347, 246  
 Lyo, A.-R., Song, I., Lawson, W. A., Bessell, M. S., & Zuckerman, B. 2006, *MNRAS*, 392  
 Mamajek, E. E., Lawson, W. A., & Feigelson, E. D. 1999, *ApJ*, 516, L77  
 —. 2000, *ApJ*, 544, 356  
 Mathieu, R. D., Ghez, A. M., Jensen, E. L. N., & Simon, M. 2000, *Protostars and Planets IV*, 703  
 Meeus, J. 1991, *Astronomical algorithms* (Willmann-Bell, Inc.)  
 Moffat, A. F. J. 1969, *A&A*, 3, 455  
 Padgett, D. L., Strom, S. E., & Ghez, A. 1997, *ApJ*, 477, 705  
 Patience, J., & Duchêne, G. 2001, in *IAU Symposium*, ed. H. Zinnecker & R. Mathieu, 181–  
 Peck, E. R., & Reeder, K. 1972, *Journal of the Optical Society of America* (1917-1983), 62, 958

<sup>2</sup> An applet to compute binomial confidence intervals is available at <http://statpages.org/confint.html>

- Petr, M. G., Coude Du Foresto, V., Beckwith, S. V. W., Richichi, A., & McCaughrean, M. J. 1998, ApJ, 500, 825
- Reipurth, B. 2000, AJ, 120, 3177
- Roe, H. G. 2002, PASP, 114, 450
- Song, I., Zuckerman, B., & Bessell, M. S. 2004, ApJ, 600, 1016
- Storer, B. E., & Kim, C. 1990, Journal of the American Statistical Association, 85, 146